

Reinforcing increase of ΔT_c in MgB₂ smart meta-superconductors by adjusting the concentration of inhomogeneous phases

Yongbo Li, Guangyu Han, Hongyan Zou, Li Tang, Honggang Chen and Xiaopeng Zhao*

Smart Materials Laboratory, Department of Applied Physics, Northwestern Polytechnical University, Xi'an 710072, China;

*Correspondence: xpzhao@nwpu.edu.cn (X.Z.)

Abstract

Incorporating with inhomogeneous phases with high electroluminescence (EL) intensity to prepare smart meta-superconductors (SMSCs) is an effective method of increasing the superconducting transition temperature (T_c) and has been confirmed in both MgB₂ and Bi(Pb)SrCaCuO systems. However, the increase of ΔT_c ($\Delta T_c = T_c - T_{c_{pure}}$) has been quite small because of the low optimal concentrations of inhomogeneous phases. In this work, three kinds of MgB₂ raw materials, namely, ^aMgB₂, ^bMgB₂, and ^cMgB₂, were prepared with particle sizes decreasing in order. Inhomogeneous phases, Y₂O₃:Eu³⁺ and Y₂O₃:Eu³⁺/Ag, were also prepared and doped into MgB₂ to study the influence of doping concentration on the ΔT_c of MgB₂ with different particle sizes. Results show that reducing the MgB₂ particle size increases the optimal doping concentration of inhomogeneous phases, thereby increasing ΔT_c . The optimal doping concentrations for ^aMgB₂, ^bMgB₂, and ^cMgB₂ are 0.5%, 0.8%, and 1.2%, respectively. The corresponding ΔT_c values are 0.4, 0.9, and 1.2 K, respectively. This work opens a new approach to reinforcing increase of ΔT_c in MgB₂ SMSCs.

Keywords: MgB₂; inhomogeneous phase; SMSCs; ΔT_c

1 Introduction

According to BCS theory, McMillan theoretically calculated the upper limit of the critical temperature (T_c) of conventional BCS superconductors to be 40 K, which is called the McMillan limit temperature [1,2]. Although the T_c of conventional superconductors has an upper limit, the search for high- T_c superconducting materials has been continuous. High-temperature superconductors [3–6], iron-based superconductors [7–10], high-pressure superconductors [11–15], and photo-induced superconductors [16,17] have been gradually studied and discovered. However, these superconducting materials are not simple conventional superconductors. Breaking the McMillan limit temperature remains a challenge for conventional BCS superconductors. In 2001, the superconductivity of MgB₂ was discovered [18]. The excellent superconductivity, simple

preparation process, and especially high T_c of MgB₂ quickly aroused great interest in the scientific community and led scholars to believe that the McMillan limit temperature may finally be surpassed [19–24]. Various methods have been applied to improve the superconductivity of MgB₂, which would not only improve the practical application of MgB₂ but also help transcend the McMillan limit temperature and further elucidate the superconducting mechanism [25–29]. Chemical doping is often used to study superconductivity. Unfortunately, many experimental results [30–35] confirm that this method reduces the T_c of MgB₂. Thus far, no useful strategy for improving the T_c of MgB₂ is yet available.

Metamaterial mainly refers to materials made up of two or more media, which can produce new properties that are not found in a single medium. Meta-method is often used to achieve some special properties and provides new ways of improving the T_c of materials [36–38]. In 2007, our group proposed a method based on the structural design of metamaterials for increasing the T_c of superconductors [39,40]. In this method, electroluminescence (EL) materials are directly doped into a superconductor to form a smart meta-superconductor (SMSC). The external field added during the measurement of the T_c of SMSC with a four-probe method can excite the inhomogeneous phases to generate EL, achieving the purpose of strengthening the Cooper pairs, resulting the change of T_c in macroscopic. A SMSC is a material whose T_c can be adjusted and improved by the stimulus of external field, which is a new property and cannot be achieved by traditional doping with a second phase [41–46]. Our group subsequently conducted a series of studies, mainly using MgB₂ as the base superconducting material and Y₂O₃:Eu³⁺ as the base EL material [41–43]. The results obtained in these studies show that unlike conventional chemical doping, which consistently reduces the T_c of MgB₂, the SMSC method of doping EL materials could help increase the T_c of MgB₂. The same conclusions were drawn from substituting the inhomogeneous phase with YVO₄:Eu³⁺ or luminescent nanocomposite Y₂O₃:Eu³⁺/Ag [44,45] and replacing MgB₂ with Bi(Pb)SrCaCuO [46]. The effectiveness of improving the T_c of superconducting materials through the SMSC method by doping with EL inhomogeneous phases has been proven, but the ΔT_c ($\Delta T_c = T_c - T_{c_{pure}}$) values obtained are generally small (0.2–0.4 K). Our previous results show that the SMSC method can only improve T_c at low concentrations of inhomogeneous phases and leads to a small ΔT_c , greatly hindering the further improvement of the T_c of MgB₂.

In this work, three types of MgB₂ raw materials, namely, ^aMgB₂, ^bMgB₂, and ^cMgB₂, were prepared with particle sizes decreasing in order. Two types of inhomogeneous phases, namely, Y₂O₃:Eu³⁺ and Y₂O₃:Eu³⁺/Ag, were also prepared based on our previous preparation method [47,48]. Two other types of non-EL dopants, namely, Y₂O₃ and Y₂O₃:Sm³⁺, were also prepared for comparison. These four types of dopants were incorporated into MgB₂, and the change of T_c was studied. The results show that the T_c of MgB₂ doped with non-EL Y₂O₃ and Y₂O₃:Sm³⁺ is lower than that of pure MgB₂ ($\Delta T_c < 0$). By contrast, EL inhomogeneous phases Y₂O₃:Eu³⁺ and Y₂O₃:Eu³⁺/Ag increase the T_c ($\Delta T_c > 0$), and the optimal doping concentration of the inhomogeneous phases increased from 0.5% to 1.2% with the decrease of MgB₂'s particle size. The optimal doping concentrations for ^aMgB₂, ^bMgB₂, and ^cMgB₂ are 0.5%, 0.8%, and 1.2%, respectively. The corresponding ΔT_{cs} are 0.4, 0.9, and 1.2 K, which exhibit significant improvements compared with the ΔT_{cs} (0.2–0.4 K) in previous work [41–45].

2 Model

Figure 1a–c show the cross-sectional view of MgB₂ SMSCs models prepared using ^aMgB₂ ($\Phi_a < 30 \mu\text{m}$), ^bMgB₂ ($\Phi_b < 15 \mu\text{m}$), and ^cMgB₂ ($\Phi_c < 5 \mu\text{m}$) as raw materials. Φ_a , Φ_b , and Φ_c refer to the particle sizes of ^aMgB₂, ^bMgB₂, and ^cMgB₂ powders, which will be described in detail at the experiment section. The brown hexagons represent the MgB₂ particles, and the gray dashed lines represent the flakes of inhomogeneous phase with the surface size of approximately 20 nm and thickness of approximately 2.5 nm [45,48]. The flakes of Y₂O₃, Y₂O₃:Sm³⁺, Y₂O₃:Eu³⁺, and Y₂O₃:Eu³⁺/Ag mainly gather on the surfaces of the MgB₂ particles as shown in Figure 1d. Figure 1e–h present the schematics of Y₂O₃, Y₂O₃:Sm³⁺, Y₂O₃:Eu³⁺, and Y₂O₃:Eu³⁺/Ag, respectively. The gray flake represents Y₂O₃. The yellow, white, and green points represent Sm, Eu, and Ag. Obviously, the introduction of these four dopants inevitably reduces the T_c of MgB₂. This is mainly because the dopants are not superconductors, which is unfavorable for the superconductivity of MgB₂, like the impurity phase of MgO in MgB₂. For convenience, the reduction in T_c caused by introducing the dopants is referred to as the impurity effect [41–46]. Non-EL dopants Y₂O₃ and Y₂O₃:Sm³⁺ can only decrease T_c for the introduction of the impurity effect. Unlike Y₂O₃ and Y₂O₃:Sm³⁺, introducing EL Y₂O₃:Eu³⁺ and Y₂O₃:Eu³⁺/Ag may increase the T_c of MgB₂. In the experiment, a four-probe method is used to measure the T_c . During the measurements, the applied external electric field forms local electric fields in the superconductor, which could excite the inhomogeneous phase to produce EL. The generated EL excites the electrons in turn, which is favorable to the formation of Cooper pairs and enables the increase in T_c . This process is collectively referred to as the EL exciting effect [41–46]. A distinct competition exists between these two effects. T_c would be improved ($\Delta T_c > 0$) when EL exciting effect dominates; otherwise, introducing the inhomogeneous phase would decrease T_c ($\Delta T_c < 0$). During the preparation process, the impurity effect should be reduced as extensively as possible, and the EL exciting effect should be enhanced to obtain samples with a high T_c . The resulting superconductor is called a SMSC, and the T_c of which can be improved and adjusted by incorporating EL inhomogeneous phases [41–46].

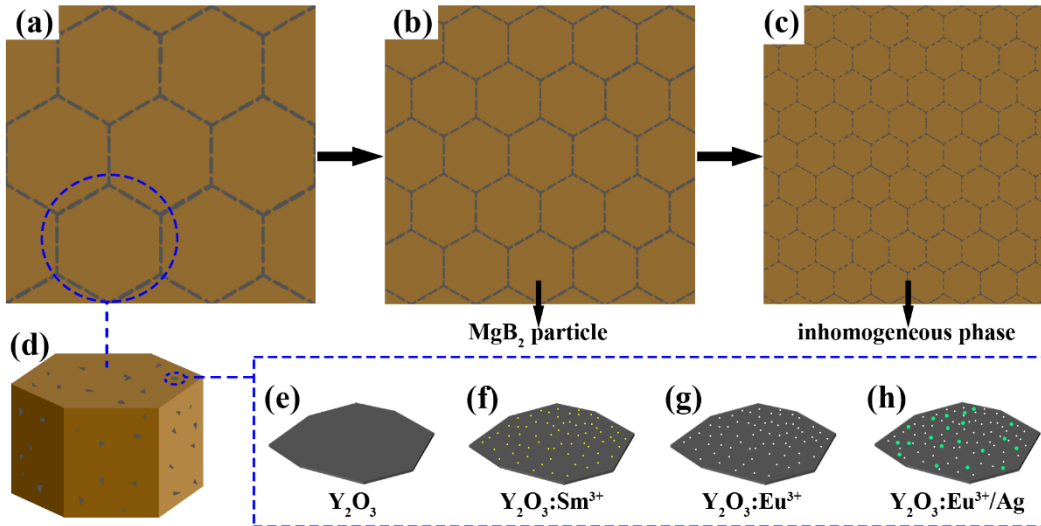


Fig. 1 The models of MgB₂ SMSCs prepared using (a) ^aMgB₂ ($\Phi_a < 30 \mu\text{m}$), (b) ^bMgB₂ ($\Phi_b < 15 \mu\text{m}$), and (c) ^cMgB₂ ($\Phi_c < 5 \mu\text{m}$) as raw materials. Schematic depictions of (d) a particle of MgB₂ SMSC, (e) Y₂O₃, (f) Y₂O₃:Sm³⁺, (g) Y₂O₃:Eu³⁺, and (h) Y₂O₃:Eu³⁺/Ag. The morphology of Y₂O₃, Y₂O₃:Sm³⁺, Y₂O₃:Eu³⁺, and Y₂O₃:Eu³⁺/Ag is flaky with surface size of approximately 20 nm and thickness of approximately 2.5 nm [45].

However, the ΔT_{cs} obtained in our previous work through the SMSC method are quite small. The low doping concentrations of inhomogeneous phases greatly hindered the further improvement of T_c . To further improve the ΔT_c of MgB_2 , the doping concentration of the inhomogeneous phase must be increased to enhance the EL exciting effect. However, the impurity effect inevitably increases with the increasing doping concentration, as analyzed above. The results of our previous work show that the impurity effect tends to dominate at high concentrations, which is not conducive to the T_c of the sample. This phenomenon is principally caused by the agglomeration of excessive inhomogeneous phase flakes, which cannot disperse well in the sample to improve T_c at concentrations exceeding the optimal value. A simple strategy to solve this problem is to reduce the particle size of MgB_2 as shown in Figure 1a–c. It can be seen that reducing the particle size would increase the region between the particles, thereby increasing the optimal doping concentration of the inhomogeneous phase. The inhomogeneous phase flakes can disperse well in the sample with small particle size and fully exert the EL exciting effect to further increase ΔT_c .

3 Experiment

Y_2O_3 , $\text{Y}_2\text{O}_3:\text{Sm}^{3+}$, $\text{Y}_2\text{O}_3:\text{Eu}^{3+}$, and $\text{Y}_2\text{O}_3:\text{Eu}^{3+}/\text{Ag}$ were prepared by a hydrothermal method [47,48]. Briefly, a certain amount of Y_2O_3 and Eu_2O_3 were weighed and dissolved in HCl to make a precursor. The precursor was dissolved in benzyl alcohol and stirred on a magnetic stirrer. A certain amount of octylamine and AgNO_3 was added dropwise into the beaker in turn. Then the mixture was transferred to a high-pressure reaction kettle, which was then placed in a drying oven and kept at 250 °C for 24 h. Thereafter, the reaction kettle was naturally cooled to room temperature. The precipitate was washed several times with absolute ethanol to remove impurities and then separated from the solution by centrifugation, precipitation, and drying. The obtained solids were placed in a high-temperature tube furnace and heated at 800 °C for 24 h to form a white powder. After illumination, $\text{Y}_2\text{O}_3:\text{Eu}^{3+}/\text{Ag}$ was obtained. The same procedure was carried out to prepare Y_2O_3 , $\text{Y}_2\text{O}_3:\text{Eu}^{3+}$, and $\text{Y}_2\text{O}_3:\text{Sm}^{3+}$ by controlling the addition of Eu_2O_3 and AgNO_3 and replacing Eu_2O_3 with Sm_2O_3 . The morphology of Y_2O_3 , $\text{Y}_2\text{O}_3:\text{Sm}^{3+}$, $\text{Y}_2\text{O}_3:\text{Eu}^{3+}$, and $\text{Y}_2\text{O}_3:\text{Eu}^{3+}/\text{Ag}$ is flaky with surface size of approximately 20 nm and thickness of approximately 2.5 nm [45,48].

Three types of MgB_2 raw materials marked with $^a\text{MgB}_2$, $^b\text{MgB}_2$, and $^c\text{MgB}_2$ were prepared in this work. Φ_a , Φ_b , and Φ_c refer to the particle sizes of $^a\text{MgB}_2$, $^b\text{MgB}_2$, and $^c\text{MgB}_2$ powders. A 500-mesh sieve was used to sift MgB_2 powder (99%, 100 mesh, Alfa Aesar) to prepare $^a\text{MgB}_2$, indicating that $\Phi_a < 30 \mu\text{m}$. $^b\text{MgB}_2$ was prepared by sifting $^a\text{MgB}_2$ powder through vacuum filtration with the pore size of about 15 μm , indicating that $\Phi_b < 15 \mu\text{m}$. Meanwhile, Mg and nano boron powder sifted through vacuum filtration with the pore size of about 5 μm were applied to prepare MgB_2 powder by the traditional sintering process. The obtained MgB_2 powder was then sifted through vacuum filtration with the pore size of about 5 μm to prepare $^c\text{MgB}_2$, indicating that $\Phi_c < 5 \mu\text{m}$. MgB_2 -based superconductors were synthesized by an ex situ preparation process, which is described in detail in our previous work [42,45]. The doping concentrations in this work all refer to the mass percentage.

4 Results and discussion

Figure 2a shows the EL spectra of Y_2O_3 , $\text{Y}_2\text{O}_3:\text{Sm}^{3+}$, $\text{Y}_2\text{O}_3:\text{Eu}^{3+}$, and $\text{Y}_2\text{O}_3:\text{Eu}^{3+}/\text{Ag}$, which confirm that Y_2O_3 and $\text{Y}_2\text{O}_3:\text{Sm}^{3+}$ are non-EL materials, whereas $\text{Y}_2\text{O}_3:\text{Eu}^{3+}$ and $\text{Y}_2\text{O}_3:\text{Eu}^{3+}/\text{Ag}$ show a remarkable EL property. Among the four materials tested, $\text{Y}_2\text{O}_3:\text{Eu}^{3+}/\text{Ag}$ showed the highest EL intensity because of the composite luminescence [47]. Figure 2b–d present the SEM images of the pure MgB_2 samples prepared using three different raw materials. Figure 2b is the SEM image of $^a\text{MgB}_2$, which shows that most of the particle exceeded 1 μm . For $^b\text{MgB}_2$, only a few of the particles exceeded 1 μm as shown in Figure 2c. Figure 2d presents the SEM image of $^c\text{MgB}_2$, which shows that most of particles are below 500 nm. The particle sizes of $^a\text{MgB}_2$, $^b\text{MgB}_2$, and $^c\text{MgB}_2$ samples decrease in order. Figure 2e reveals the XRD patterns of four samples. The black and red curves depict the XRD patterns of $^a\text{MgB}_2$ and $^a\text{MgB}_2+0.5\% \text{Y}_2\text{O}_3:\text{Eu}^{3+}/\text{Ag}$, respectively. The blue and magenta curves correspond to the XRD patterns of $^b\text{MgB}_2+0.8\% \text{Y}_2\text{O}_3:\text{Eu}^{3+}/\text{Ag}$ and $^c\text{MgB}_2+1.2\% \text{Y}_2\text{O}_3:\text{Eu}^{3+}/\text{Ag}$, respectively. The black vertical lines represent the standard XRD patterns of MgB_2 . The main phase of all the samples was clearly MgB_2 . The Y_2O_3 phase was found in the doped samples. Small amounts of the unavoidable MgO phase were also detected in all the samples [49–52]. The XRD patterns of the other samples show a similar feature.

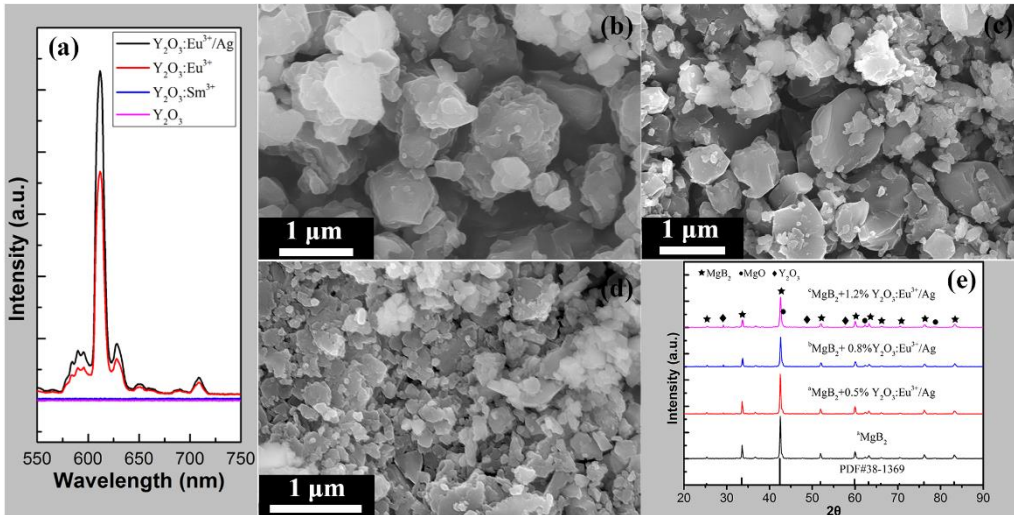


Fig. 2 (a) EL intensities of Y_2O_3 , $\text{Y}_2\text{O}_3:\text{Sm}^{3+}$, $\text{Y}_2\text{O}_3:\text{Eu}^{3+}$, and $\text{Y}_2\text{O}_3:\text{Eu}^{3+}/\text{Ag}$. (b–d) SEM images of $^a\text{MgB}_2$, $^b\text{MgB}_2$, and $^c\text{MgB}_2$, respectively. (e) XRD patterns of $^a\text{MgB}_2$, $^a\text{MgB}_2+0.5\% \text{Y}_2\text{O}_3:\text{Eu}^{3+}/\text{Ag}$, $^b\text{MgB}_2+0.8\% \text{Y}_2\text{O}_3:\text{Eu}^{3+}/\text{Ag}$, and $^c\text{MgB}_2+1.2\% \text{Y}_2\text{O}_3:\text{Eu}^{3+}/\text{Ag}$.

Figure 3a illustrates the normalized resistivity-temperature ($R-T$) curves of $^a\text{MgB}_2$ doped with $x\% \text{Y}_2\text{O}_3$ ($x = 0, 0.2, 0.5, 0.8, 1.0, 1.2$). The black curve corresponds to the $^a\text{MgB}_2$ sample, which shows that the T_c of the pure sample was 37.4–38.2 K. The onset and offset critical temperatures of pure $^a\text{MgB}_2$ are 38.2 K and 37.4 K. The other curves represent $^a\text{MgB}_2$ doped with Y_2O_3 with concentrations of 0.2%, 0.5%, 0.8%, 1.0%, and 1.2%, indicating that the corresponding T_{cs} are 37.0–37.8 K, 36.8–37.6 K, 36.5–37.3 K, 36.1–37.0 K, and 35.8–36.8 K. The results show that like conventional chemical doping, the introduction of non-EL Y_2O_3 decreases the T_c of MgB_2 ($\Delta T_c < 0$) and the T_{cs} of the doped samples decrease with the increase of the doping concentration as shown in the inset figure. Figure 3b shows the normalized $R-T$ curves of $^a\text{MgB}_2$ doped with 0.5% y ($y = 0, \text{Y}_2\text{O}_3, \text{Y}_2\text{O}_3:\text{Sm}^{3+}, \text{Y}_2\text{O}_3:\text{Eu}^{3+}, \text{Y}_2\text{O}_3:\text{Eu}^{3+}/\text{Ag}$). The doping concentration was fixed at 0.5% base on

our previous work [45]. The T_c values of MgB₂ doped with Y₂O₃, Y₂O₃:Sm³⁺, Y₂O₃:Eu³⁺, and Y₂O₃:Eu³⁺/Ag were 36.8–37.6 K, 36.9–37.7 K, 37.6–38.4 K, and 37.8–38.6 K. The results clearly show that non-EL Y₂O₃ and Y₂O₃:Sm³⁺ decreased the T_c of MgB₂, while EL Y₂O₃:Eu³⁺ and Y₂O₃:Eu³⁺/Ag increased the T_c of MgB₂, as shown in the inset. The T_c values of MgB₂ doped with Y₂O₃:Eu³⁺ and Y₂O₃:Eu³⁺/Ag increased by 0.2 and 0.4 K, respectively, compared with that of ^aMgB₂. This finding is similar to those of our previous studies.

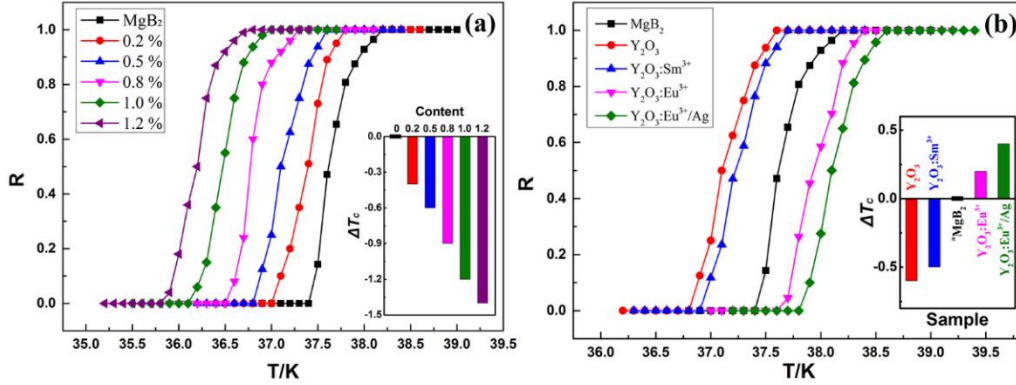


Fig. 3 Normalized resistivity-temperature curves of ^aMgB₂ doped with (a) $x\%$ Y₂O₃ ($x = 0, 0.2, 0.5, 0.8, 1.0, 1.2$) and (b) 0.5% y ($y = 0, \text{Y}_2\text{O}_3, \text{Y}_2\text{O}_3:\text{Sm}^{3+}, \text{Y}_2\text{O}_3:\text{Eu}^{3+}, \text{Y}_2\text{O}_3:\text{Eu}^{3+}/\text{Ag}$). Insets: the values of ΔT_c ($\Delta T_c = T_c - T_{c\text{pure}}$).

Figure 4a illustrates the normalized R – T curves of ^bMgB₂ doped with $x\%$ Y₂O₃:Eu³⁺ ($x = 0, 0.5, 0.6, 0.7, 0.8, 1.0$). The black curve corresponds to ^bMgB₂, which shows that the T_c of the pure sample is 36.6–37.4 K. The other curves are the R – T curves of ^bMgB₂ doped with Y₂O₃:Eu³⁺ with doping concentrations of 0.5%, 0.6%, 0.7%, 0.8%, 0.9%, and 1.0%, indicating that the corresponding T_{cs} are 36.8–37.6 K, 37–37.8 K, 37.2–38.0 K, 37.4–38.2 K, 37.0–37.9 K, and 36.7–37.7 K. The T_c of the doped samples first increased and then decreased with the increase of the doping concentration. The inset summarizes the evolution of ΔT_c as a function of the doping concentration. The optimal doping concentration and the corresponding ΔT_c increased to 0.8% and 0.8 K, respectively, compared with those of the samples prepared using ^aMgB₂ as raw material. Figure 4b demonstrates the normalized R – T curves of ^bMgB₂ doped with 0.8% y ($y = 0, \text{Y}_2\text{O}_3, \text{Y}_2\text{O}_3:\text{Sm}^{3+}, \text{Y}_2\text{O}_3:\text{Eu}^{3+}, \text{Y}_2\text{O}_3:\text{Eu}^{3+}/\text{Ag}$). The T_{cs} of ^bMgB₂ doped with Y₂O₃, Y₂O₃:Sm³⁺, Y₂O₃:Eu³⁺, and Y₂O₃:Eu³⁺/Ag were 35.8–36.6 K, 36.0–36.8 K, 37.4–38.2 K, and 37.5–38.3 K, respectively. Among these samples, ^bMgB₂+0.8% Y₂O₃:Eu³⁺/Ag obtained the highest ΔT_c (0.9 K) because of the high EL intensity, as shown in Figure 2a.

Figure 4c reveals the normalized R – T curves of ^cMgB₂ doped with $x\%$ Y₂O₃:Eu³⁺ ($x = 0, 0.8, 1.0, 1.2, 1.5$). Similarly, the black curve corresponds to the pure sample, indicating that the T_c of ^cMgB₂ is 36.0–36.8 K. The other curves correspond to ^cMgB₂ doped with Y₂O₃:Eu³⁺ at different concentrations of 0.8%, 1.0%, 1.2%, and 1.5%, indicating that the corresponding T_{cs} are 36.2–37.0 K, 36.6–37.4 K, 37.0–37.8 K, and 36.4–37.2 K, respectively. It is same with the results in Figure 4a, that is, T_c first increases and then decreases with the increase of the doping concentration, as shown in the inset figure. The optimal doping concentration is 1.2%, and the corresponding ΔT_c is 1.0 K. Figure 4d shows the normalized R – T curves of ^cMgB₂ doped with 1.2% y ($y = 0, \text{Y}_2\text{O}_3, \text{Y}_2\text{O}_3:\text{Sm}^{3+}, \text{Y}_2\text{O}_3:\text{Eu}^{3+}, \text{Y}_2\text{O}_3:\text{Eu}^{3+}/\text{Ag}$). The T_c values of ^cMgB₂ doped with Y₂O₃, Y₂O₃:Sm³⁺, Y₂O₃:Eu³⁺, Y₂O₃:Eu³⁺/Ag are 34.7–35.7 K, 34.9–35.7 K, 37.0–37.8 K, and 37.2–38.0 K. Y₂O₃ and Y₂O₃:Sm³⁺

decrease T_c , whereas $\text{Y}_2\text{O}_3:\text{Eu}^{3+}$ and $\text{Y}_2\text{O}_3:\text{Eu}^{3+}/\text{Ag}$ increase T_c . These results are consistent with those of the samples prepared using $^a\text{MgB}_2$ and $^b\text{MgB}_2$ as raw materials. The T_c of $^c\text{MgB}_2+1.2\%$ $\text{Y}_2\text{O}_3:\text{Eu}^{3+}/\text{Ag}$ was enhanced by 1.2 K compared with that of the pure sample, exhibiting the highest ΔT_c among the samples.

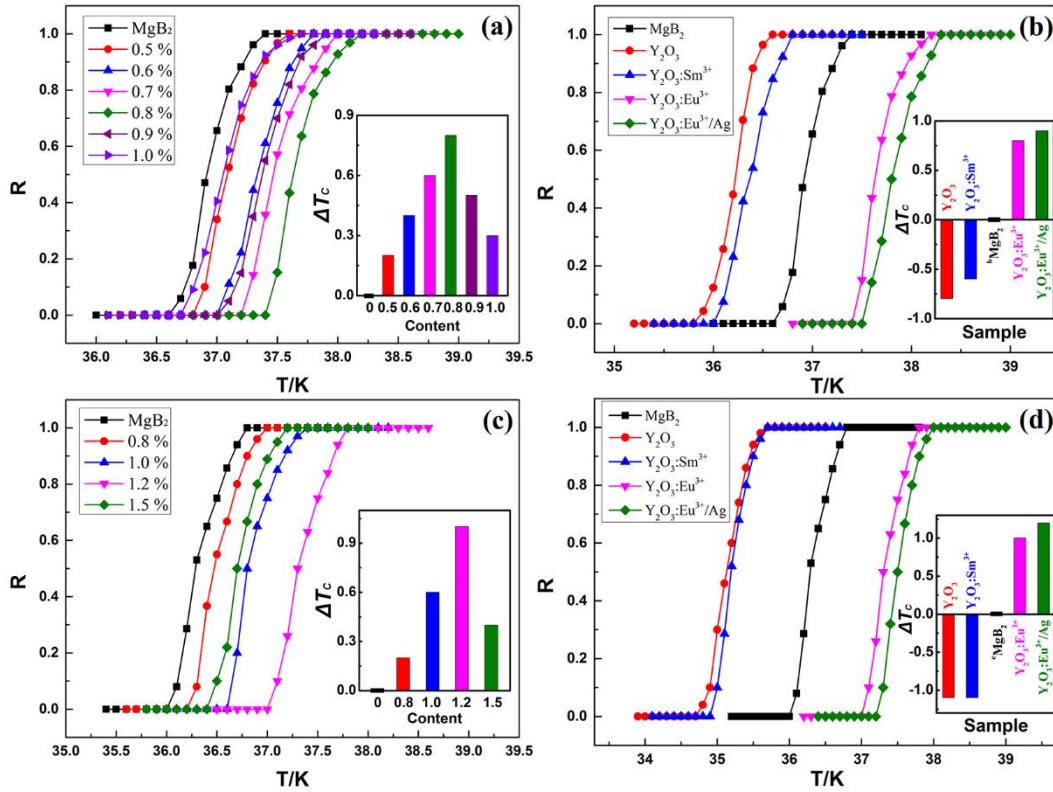


Fig. 4 Normalized $R-T$ curves of $^b\text{MgB}_2$ doped with (a) $x\%$ $\text{Y}_2\text{O}_3:\text{Eu}^{3+}$ ($x = 0, 0.5, 0.6, 0.7, 0.8, 0.9, 1.0$) and (b) 0.8% y ($y = 0, \text{Y}_2\text{O}_3, \text{Y}_2\text{O}_3:\text{Sm}^{3+}, \text{Y}_2\text{O}_3:\text{Eu}^{3+}, \text{Y}_2\text{O}_3:\text{Eu}^{3+}/\text{Ag}$). Normalized $R-T$ curves of $^c\text{MgB}_2$ doped with (c) $x\%$ $\text{Y}_2\text{O}_3:\text{Eu}^{3+}$ ($x = 0, 0.8, 1.0, 1.2, 1.5$) and (d) 1.2% y ($y = 0, \text{Y}_2\text{O}_3, \text{Y}_2\text{O}_3:\text{Sm}^{3+}, \text{Y}_2\text{O}_3:\text{Eu}^{3+}, \text{Y}_2\text{O}_3:\text{Eu}^{3+}/\text{Ag}$). Insets: the values of ΔT_c ($\Delta T_c = T_c - T_{c\text{pure}}$).

Figure 5a shows the SEM image of $^a\text{MgB}_2+0.5\%$ $\text{Y}_2\text{O}_3:\text{Eu}^{3+}/\text{Ag}$. Figure 5b–e are the EDS mapping for elements Mg, Y, Eu, and Ag listed in the lower right corner of each figure. Figure 5f shows the SEM image of $^c\text{MgB}_2+1.2\%$ $\text{Y}_2\text{O}_3:\text{Eu}^{3+}/\text{Ag}$. Figure 5g–j are the EDS mapping for elements Mg, Y, Eu, and Ag. Given that the inhomogeneous phase did not react with MgB_2 , the mapping of elements Y, Eu, and Ag can reflect the distribution of the inhomogeneous phase in the sample. It can be seen that $\text{Y}_2\text{O}_3:\text{Eu}^{3+}/\text{Ag}$ is relatively evenly distributed in $^a\text{MgB}_2$. Similarly, the inhomogeneous phase did not generate significant agglomeration in $^c\text{MgB}_2$, even though the optimal concentration was enhanced to 1.2% as the particle size decreased, as shown in Figure 5g–j. Therefore, the inhomogeneous phase was able to fully exert the EL exciting effect to further increase ΔT_c at high concentrations.

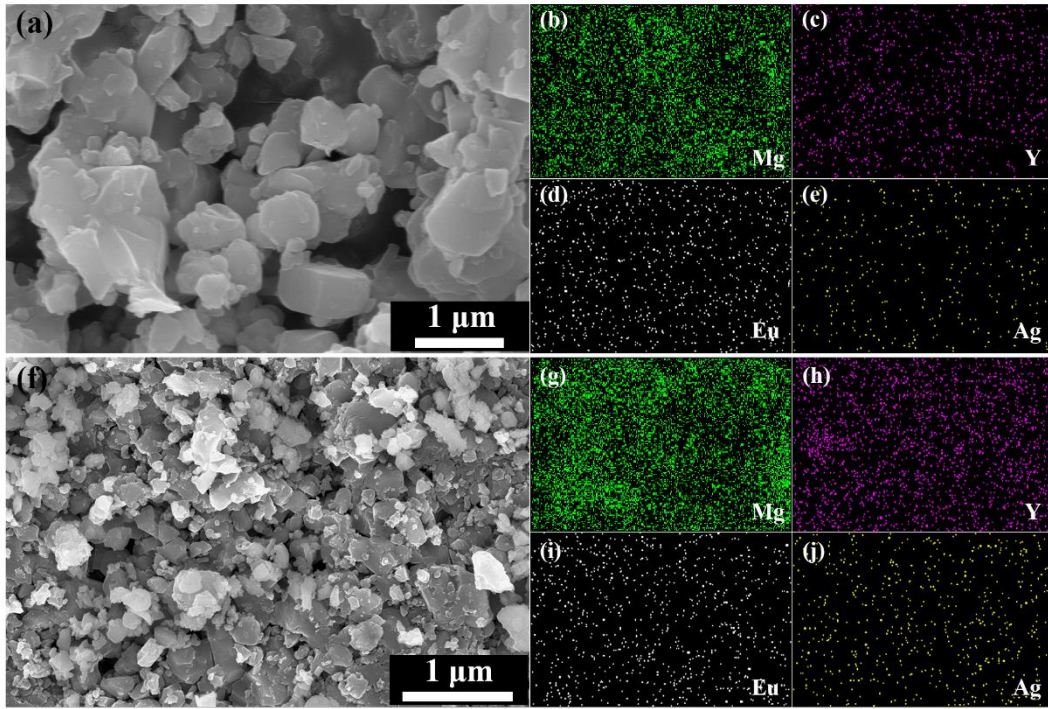


Fig. 5 (a) SEM image and (b–e) EDS mapping of ^aMgB₂+0.5% Y₂O₃:Eu³⁺/Ag. (f) SEM image and (g–j) EDS mapping of ^cMgB₂+1.2% Y₂O₃:Eu³⁺/Ag.

Table 1 shows the ΔT_{cs} for ^aMgB₂+0.5% x , ^bMgB₂+0.8% x and ^cMgB₂+1.2% x ($x = \text{Y}_2\text{O}_3$, $\text{Y}_2\text{O}_3:\text{Sm}^{3+}$, $\text{Y}_2\text{O}_3:\text{Eu}^{3+}$, and $\text{Y}_2\text{O}_3:\text{Eu}^{3+}/\text{Ag}$). For the ^aMgB₂ raw material, we prepared the MgB₂ SMSCs doped with 0.5% inhomogeneous phase. The results show that ΔT_c values for ^aMgB₂ doped with $\text{Y}_2\text{O}_3:\text{Eu}^{3+}$ and $\text{Y}_2\text{O}_3:\text{Eu}^{3+}/\text{Ag}$ are 0.2 K and 0.4 K. For the ^bMgB₂ raw material with a smaller particle size than that of ^aMgB₂, the optimal doping concentration was first explored by changing the concentration of $\text{Y}_2\text{O}_3:\text{Eu}^{3+}$ from 0.5% to 1.0%. The results show that the optimal doping concentration is 0.8%. Subsequently, 0.8% Y_2O_3 , $\text{Y}_2\text{O}_3:\text{Sm}^{3+}$, $\text{Y}_2\text{O}_3:\text{Eu}^{3+}$, and $\text{Y}_2\text{O}_3:\text{Eu}^{3+}/\text{Ag}$ were separately doped into ^bMgB₂ to study the change of T_c . The results clearly show that Y_2O_3 and $\text{Y}_2\text{O}_3:\text{Sm}^{3+}$ reduced T_c , whereas $\text{Y}_2\text{O}_3:\text{Eu}^{3+}$ and $\text{Y}_2\text{O}_3:\text{Eu}^{3+}/\text{Ag}$ enhanced T_c , and the corresponding ΔT_c values were 0.8 K and 0.9 K, respectively. Similar results were obtained in the samples prepared using ^cMgB₂ as the raw material. For ^cMgB₂, which has the smallest particle size among the three raw materials, the optimal concentration was enhanced to 1.2%. The ΔT_{cs} for ^cMgB₂ doped with $\text{Y}_2\text{O}_3:\text{Eu}^{3+}$ and $\text{Y}_2\text{O}_3:\text{Eu}^{3+}/\text{Ag}$ were 1.0 K and 1.2 K, respectively. These results indicate that reducing the particle to increase the region between the particles can effectively enhance the optimal doping concentration, thereby enhancing the ΔT_c .

Table 1 ΔT_{cs} for ^aMgB₂+0.5% x , ^bMgB₂+0.8% x and ^cMgB₂+1.2% x ($x = \text{Y}_2\text{O}_3$, $\text{Y}_2\text{O}_3:\text{Sm}^{3+}$, $\text{Y}_2\text{O}_3:\text{Eu}^{3+}$, and $\text{Y}_2\text{O}_3:\text{Eu}^{3+}/\text{Ag}$).

	Y_2O_3	$\text{Y}_2\text{O}_3:\text{Sm}^{3+}$	$\text{Y}_2\text{O}_3:\text{Eu}^{3+}$	$\text{Y}_2\text{O}_3:\text{Eu}^{3+}/\text{Ag}$
^a MgB ₂ (0.5%)	-0.6 K	-0.5 K	0.2 K	0.4 K
^b MgB ₂ (0.8%)	-0.8 K	-0.6 K	0.8 K	0.9 K
^c MgB ₂ (1.2%)	-1.1 K	-1.1 K	1.0 K	1.2 K

In this work, the ΔT_c is improved by increasing the optimal doping concentration of inhomogeneous phases through reducing the particle size, however, the T_c values of MgB₂ SMSCs are relatively low due to the low T_c of the pure MgB₂ sample. As the particle size decreases, the grain boundaries in the sample increase and the connectivity decreases, which are disadvantages to the superconductivity [53–55]. One possible solution is to incorporate the inhomogeneous phase into the interior of the particles to overcome the disadvantages caused by the increasing grain boundaries with the doping concentration increasing.

5 Conclusions

Although the effectiveness of improving the T_c of superconducting materials through the SMSC method by doping with EL inhomogeneous phases has been proven in previous works, the ΔT_{cs} obtained are quite small. To further increase ΔT_c , three types of MgB₂ raw materials, namely, ^aMgB₂, ^bMgB₂, and ^cMgB₂, were prepared with particle sizes decreasing in order. EL inhomogeneous phases were incorporated into these three raw materials with different concentrations to study the change of ΔT_c . The results show that the optimal doping concentrations for ^aMgB₂, ^bMgB₂, and ^cMgB₂ are 0.5%, 0.8%, and 1.2%, respectively. The corresponding ΔT_{cs} are 0.4, 0.9, and 1.2 K, respectively. Meanwhile, increasing the EL intensity of the inhomogeneous phase can be considered to further increase ΔT_c . This work not only proves the effectiveness of the SMSC method in improving T_c but also provides an alternative approach to improving the T_c of superconducting materials.

Acknowledgement

This work was supported by the National Natural Science Foundation of China for Distinguished Young Scholar under Grant No.50025207.

Reference

1. J. Bardeen, L. N. Cooper, J. R. Schrieffer, Theory of Superconductivity. *Phys. Rev.* **108**, 1175–1204 (1957)
2. W. L. McMillan, Transition Temperature of Strong-Coupled Superconductors. *Phys. Rev.* **167**, 331–344 (1968)
3. J. G. Bednorz, K. A. Müller, Possible high T_c superconductivity in the Ba-La-Cu-O system. *Z. Phys. B - Condensed Matter* **64**, 189–193 (1986)
4. C. W. Chu, P. H. Hor, R. L. Meng, L. Gao, Z. J. Huang, Y. Q. Wang, Evidence for superconductivity above 40 K in the La-Ba-Cu-O compound system. *Phys. Rev. Lett.* **58**, 405–407 (1987)
5. S. N. Putilin, E. V. Antipov, O. Chmaissem, M. Marezio, Superconductivity at 94 K in HgBa₂CuO_{4+δ}. *Nature* **362**, 226–228 (1993)
6. N. Loudhaief, M. Ben Salem, Structural, optical and electrical studies of Bi₂S₃ nanoparticles and their impact on the superconducting properties of (Bi,Pb)₂Sr₂Ca₂Cu₃O₈ ceramics. *Appl. Phys. A* **127**, (2021)
7. X. H. Chen, T. Wu, G. Wu, R. H. Liu, H. Chen, D. F. Fang, Superconductivity at 43 K in SmFeAsO_{1-x}F_x. *Nature* **453**, 761–762 (2008)

8. Y. Kamihara, T. Watanabe, M. Hirano, H. Hosono, Iron-Based Layered Superconductor $\text{La}[\text{O}_{1-x}\text{F}_x]\text{FeAs}$ ($x = 0.05\text{--}0.12$) with $T_c = 26$ K. *J. Am. Chem. Soc.* **130**, 3296–3297 (2008)
9. Z. A. Ren, W. Lu, J. Yang, W. Yi, X. L. Shen, Z. C. Li, G. C. Che, X. L. Dong, L. L. Sun, F. Zhou, Z. X. Zhao, Superconductivity at 55 K in Iron-Based F-Doped Layered Quaternary Compound $\text{Sm}[\text{O}_{1-x}\text{F}_x]\text{FeAs}$. *Chinese Phys. Lett.* **25**, 2215–2216 (2008)
10. A. Tsukada, K. E. Luna, R. H. Hammond, M. R. Beasley, J. F. Zhao, S. H. Risbud, Pulsed laser deposition conditions and superconductivity of FeSe thin films. *Appl. Phys. A* **104**, 311–318 (2011)
11. A. P. Drozdov, M. I. Erements, I. A. Troyan, V. Ksenofontov, S. I. Shylin, Conventional superconductivity at 203 kelvin at high pressures in the sulfur hydride system. *Nature* **525**, 73–76 (2015)
12. A. Cantaluppi, M. Buzzi, G. Jotzu, D. Nicoletti, M. Mitrano, D. Pontiroli, M. Ricco, A. Perucchi, P. Di Pietro, A. Cavalleri, Pressure tuning of light-induced superconductivity in K_3C_{60} . *Nat. Phys.* **14**, 837–841 (2018)
13. A. P. Drozdov, P. P. Kong, V. S. Minkov, S. P. Besedin, M. A. Kuzovnikov, S. Mozaffari, L. Balicas, F. F. Balakirev, D. E. Graf, V. B. Prakapenka, E. Greenberg, D. A. Knyazev, M. Tkacz, M. I. Erements, Superconductivity at 250 K in lanthanum hydride under high pressures. *Nature* **569**, 528–531 (2019)
14. Y. Sun, J. Lv, Y. Xie, H. Liu, Y. Ma, Route to a Superconducting Phase above Room Temperature in Electron-Doped Hydride Compounds under High Pressure. *Phys. Rev. Lett.* **123**, 097001 (2019)
15. E. Snider, N. Dasenbrock-Gammon, R. McBride, M. Debessai, H. Vindana, K. Vencatasamy, K. V. Lawler, A. Salamat, R. P. Dias, Room-temperature superconductivity in a carbonaceous sulfur hydride. *Nature* **586**, 373–377 (2020)
16. D. Fausti, R. I. Tobey, N. Dean, S. Kaiser, A. Dienst, M. C. Hoffmann, S. Pyon, T. Takayama, H. Takagi, A. Cavalleri, Light-Induced Superconductivity in a Stripe-Ordered Cuprate. *Science* **331**, 189–191 (2011)
17. A. Cavalleri, Photo-induced superconductivity. *Contemp. Phys.* **59**, 31–46 (2017)
18. J. Nagamatsu, N. Nakagawa, T. Muranaka, Y. Zenitani, J. Akimitsu, Superconductivity at 39 K in magnesium diboride. *Nature* **410**, 63–64 (2001)
19. K. P. Bohnen, R. Heid, B. Renker, Phonon dispersion and electron-phonon coupling in MgB_2 and AlB_2 . *Phys. Rev. Lett.* **86**, 5771–5774 (2001)
20. C. Buzea, T. Yamashita, Review of the superconducting properties of MgB_2 . *Supercond. Sci. Technol.* **14**, R115–R146 (2001)
21. T. Yildirim, O. Gulseren, J. W. Lynn, C. M. Brown, T. J. Udovic, Q. Huang, N. Rogado, K. A. Regan, M. A. Hayward, J. S. Slusky, T. He, M. K. Haas, P. Khalifah, K. Inumaru, R. J. Cava, Giant anharmonicity and nonlinear electron-phonon coupling in MgB_2 : a combined first-principles calculation and neutron scattering study. *Phys. Rev. Lett.* **87**, 037001 (2001)
22. P. P. Singh, From E_{2g} to other modes: effects of pressure on electron-phonon interaction in MgB_2 . *Phys. Rev. Lett.* **97**, 247002 (2006)
23. K. Vinod, N. Varghese, U. Syamaprasad, Superconductivity of MgB_2 in the BCS framework with emphasis on extrinsic effects on critical temperature. *Supercond. Sci. Technol.* **20**, R31–R45 (2007)
24. A. Varilci, D. Yegen, M. Tassi, D. Stamopoulos, C. Terzioglu, Effect of annealing temperature on some physical properties of MgB_2 by using the Hall probe ac-susceptibility method. *Physica B: Condensed Matter* **404**, 4054–4059 (2009)
25. Y. G. Zhao, X. P. Zhang, P. T. Qiao, H. T. Zhang, S. L. Jia, B. S. Cao, M. H. Zhu, Z. H. Han, X. L. Wang, B. L. Gu, Effect of Li doping on structure and superconducting transition temperature of

- $Mg_{1-x}Li_xB_2$. *Physica C* **361**, 91–94 (2001)
26. O. Ozturk, E. Asikuzun, S. Kaya, N. S. Koc, M. Erdem, The Effect of Ar Ambient Pressure and Annealing Duration on the Microstructure, Superconducting Properties and Activation Energies of MgB_2 Superconductors. *J. Supercond. Nov. Magn.* **30**, 1161–1169 (2016)
 27. F. Cheng, Z. Ma, C. Liu, H. Li, M. Shahriar A. Hossain, Y. Bando, Y. Yamauchi, A. Fatehmulla, W. A. Farooq, Y. Liu, Enhancement of grain connectivity and critical current density in the ex-situ sintered MgB_2 superconductors by doping minor Cu. *J. Alloy. Compd.* **727**, 1105–1109 (2017)
 28. Q. Zhao, C. Jiao, E. Zhu, Z. Zhu, Refinement of MgB_2 grains and the improvement of flux pinning in MgB_2 superconductor through nano-Ni addition. *J. Alloy. Compd.* **717**, 19–24 (2017)
 29. J. C. Grivel, K. Rubešová, Increase of the critical current density of MgB_2 superconducting bulk samples by means of methylene blue dye additions. *Physica C* **565**, 1353506 (2019)
 30. S. Y. Li, Y. M. Xiong, W. Q. Mo, R. Fan, C. H. Wang, X. G. Luo, Z. Sun, H. T. Zhang, L. Li, L. Z. Cao, X. H. Chen, Alkali metal substitution effects in $Mg_{1-x}A_xB_2$ ($A = Li$ and Na). *Physica C* **363**, 219–223 (2001)
 31. J. S. Slusky, N. Rogado, K. A. Regan, M. A. Hayward, P. Khalifah, T. He, K. Inumaru, S. M. Loureiro, M. K. Haas, H. W. Zandbergen, R. J. Cava, Loss of superconductivity with the addition of Al to MgB_2 and a structural transition in $Mg_{1-x}Al_xB_2$. *Nature* **410**, 343–345 (2001)
 32. S. X. Dou, S. Soltanian, J. Horvat, X. L. Wang, S. H. Zhou, M. Ionescu, H. K. Liu, Enhancement of the critical current density and flux pinning of MgB_2 superconductor by nanoparticle SiC doping. *Appl. Phys. Lett.* **81**, 3419–3421 (2002)
 33. G. Z. Li, M. D. Sumption, M. A. Rindfleisch, C. J. Thong, M. J. Tomsic, E. W. Collings, Enhanced higher temperature (20–30 K) transport properties and irreversibility field in nano- Dy_2O_3 doped advanced internal Mg infiltration processed MgB_2 composites. *Appl. Phys. Lett.* **105**, 112603 (2014)
 34. M. A. Susner, S. D. Bohnenstiehl, S. A. Dregia, M. D. Sumption, Y. Yang, J. J. Donovan, E. W. Collings, Homogeneous carbon doping of magnesium diboride by high-temperature, high-pressure synthesis. *Appl. Phys. Lett.* **104**, 162603 (2014)
 35. M. Shahabuddin, N. A. Madhar, N. S. Alzayed, M. Asif, Uniform Dispersion and Exfoliation of Multi-Walled Carbon Nanotubes in CNT- MgB_2 Superconductor Composites Using Surfactants. *Materials* **12**, 3044 (2019)
 36. H. Liu, X. P. Zhao, Y. Yang, Q. W. Li, J. Lv, Fabrication of Infrared Left - Handed Metamaterials via Double Template - Assisted Electrochemical Deposition. *Adv. Mater.* **20**, 2050–2054 (2008)
 37. V. N. Smolyaninova, K. Zander, T. Gresock, C. Jensen, J. C. Prestigiacomo, M. S. Osofsky, I. I. Smolyaninov, Using metamaterial nanoengineering to triple the superconducting critical temperature of bulk aluminum. *Sci. Rep.* **5**, 15777 (2015)
 38. I. I. Smolyaninov, V. N. Smolyaninova, Theoretical modeling of critical temperature increase in metamaterial superconductors. *Phys. Rev. B* **93**, 184510 (2016)
 39. W. T. Jiang, Z. L. Xu, Z. Chen, X. P. Zhao, Introduce uniformly distributed ZnO nano-defects into BSCCO superconductors by nano-composite method. *J. Funct. Mater* **38**, 157–160 (2007) in Chinese, available at <http://www.cnki.com.cn/Article/CJFDTOTAL-GNCL200701046.htm>
 40. S. H. Xu, Y. W. Zhou, X. P. Zhao, Research and Development of Inorganic Powder EL Materials. *Materials Reports* **21**, 162–166 (2007) in Chinese, available at <http://www.cnki.com.cn/Article/CJFDTotal-CLDB2007S3048.htm>
 41. Z. W. Zhang, S. Tao, G. W. Chen, X. P. Zhao, Improving the Critical Temperature of MgB_2 Superconducting Metamaterials Induced by Electroluminescence. *J. Supercond. Nov. Magn.* **29**,

- 1159–1162 (2016)
42. S. Tao, Y. B. Li, G. W. Chen, X. P. Zhao, Critical Temperature of Smart Meta-superconducting MgB₂. *J. Supercond. Nov. Magn.* **30**, 1405–1411 (2017)
 43. H. G. Chen, Y. B. Li, G. W. Chen, L. X. Xu, X. P. Zhao, The Effect of Inhomogeneous Phase on the Critical Temperature of Smart Meta-superconductor MgB₂. *J. Supercond. Nov. Magn.* **31**, 3175–3182 (2018)
 44. Y. B. Li, H. G. Chen, W. C. Qi, G. W. Chen, X. P. Zhao, Inhomogeneous Phase Effect of Smart Meta-Superconducting MgB₂. *J. Low. Temp. Phys.* **191**, 217–227 (2018)
 45. Y. B. Li, H. G. Chen, M. Z. Wang, L. X. Xu, X. P. Zhao, Smart meta-superconductor MgB₂ constructed by the dopant phase of luminescent nanocomposite. *Sci. Rep.* **9**, 14194 (2019)
 46. H. G. Chen, Y. B. Li, M. Z. Wang, G. Y. Han, M. Shi, X. P. Zhao, Smart Metastructure Method for Increasing T_c of Bi(Pb)SrCaCuO High-Temperature Superconductors. *J. Supercond. Nov. Magn.* **33**, 3015–3025 (2020)
 47. M. Z. Wang, L. X. Xu, G. W. Chen, X. P. Zhao, Topological luminophor Y₂O₃:Eu³⁺+Ag with high electroluminescence performance. *ACS Appl. Mater. Interfaces* **11**, 2328–2335 (2019)
 48. L. X. Xu, M. Z. Wang, Z. X. Liu, X. P. Zhao, Nano-topological luminophor Y₂O₃:Eu³⁺ + Ag with concurrent photoluminescence and electroluminescence. *J. Mater. Sci.: Mater. Electron.* **30**, 20243–20252 (2019)
 49. D. Eyidi, O. Eibl, T. Wenzel, K. G. Nickel, M. Giovannini, A. Saccone, Phase analysis of superconducting polycrystalline MgB₂. *Micron* **34**, 85–96 (2003)
 50. Q. Z. Shi, Y. C. Liu, Z. M. Gao, Q. Zhao, Formation of MgO whiskers on the surface of bulk MgB₂ superconductors during in situ sintering. *J. Mater. Sci.* **43**, 1438–1443 (2007)
 51. Z. Q. Ma, Y. C. Liu, Q. Z. Shi, Q. Zhao, Z. M. Gao, The improved superconductive properties of MgB₂ bulks with minor Cu addition through reducing the MgO impurity. *Physica C* **468**, 2250–2253 (2008)
 52. D. K. Singh, B. Tiwari, R. Jha, H. Kishan, V. P. S. Awana, Role of MgO impurity on the superconducting properties of MgB₂. *Physica C* **505**, 104–108 (2014)
 53. M. Dogruer, G. Yildirim, O. Ozturk, C. Terzioglu, Analysis of Indentation Size Effect on Mechanical Properties of Cu-Diffused Bulk MgB₂ Superconductor Using Experimental and Different Theoretical Models. *J. Supercond. Nov. Magn.* **26**, 101–109 (2012)
 54. S. Mizutani, A. Yamamoto, J.-i. Shimoyama, H. Ogino, K. Kishio, Self-sintering-assisted high intergranular connectivity in ball-milled ex situ MgB₂ bulks. *Supercond. Sci. Technol.* **27**, 114001 (2014)
 55. O. Ozturk, E. Asikuzun, S. Kaya, Significant change in micro mechanical, structural and electrical properties of MgB₂ superconducting ceramics depending on argon ambient pressure and annealing duration. *J. Mater. Sci.: Mater. Electron.* **26**, 3840–3852 (2015)